Controls on Palaeogene deep-sea diatom-bearing sediment deposition and comparison with shallow marine environments

Cécile Figus[1,2], Johan Renaudie[3], Or M. Bialik[4,5], and Jakub Witkowski[1]

[1]Institute of Marine and Environmental Sciences, University of Szczecin, 70-383 Szczecin, Poland
[2]Doctoral School, University of Szczecin, 70-383 Szczecin, Poland
[3]FB1 Dynamik der Natur, Museum für Naturkunde, 10115 Berlin, Germany
[4]Institute of Geology and Palaeontology, University of Münster, 48149 Münster, Germany
[5]Dr. Moses Strauss Department of Marine Geosciences, The Leon H. Charney School of Marine Sciences, University of Haifa, Mount Carmel, 31905 Haifa, Israel

Correspondence: Cécile Figus (cecile.figus@phd.usz.edu.pl)

Abstract. Diatoms are the key players in the present-day global biogeochemical cycles. Yet, the diatom flux response to the dynamically changing climates of the Palaeogene has long been a subject to divergent interpretations. We present a compilation of Palaeogene deep-sea diatom-bearing sediments in order to gain new insight into inter-basin and latitudinal distribution of diatom accumulation zones from the K/Pg boundary to the Oligocene/Miocene transition. Our dataset includes 189 sites drilled

5   in the Atlantic, Pacific, and Indian oceans, and in the Arctic. It suggests that the number and distribution of deep-sea diatom-bearing sediment occurrences is mainly controlled by the nutrient availibility and ocean circulation. Climate appears to have only an indirect correlation with our results, which may be linked to the expansion of the Antarctic Ice Sheet during the Oligocene global cooling. A comparison of our results with the temporal ditribution of shallow marine diatomite occurrences (Figus et al., 2024a) suggests that the increase in the number of deep-sea diatom-bearing sediment occurrences (particularly

10   in the Atlantic) during the diatomite gap (~46 to ~44 Ma) is probably related to the tectonic reorganizations occurring during this period. These palaeogeographic changes caused the cessation of shallow marine diatomite deposition, and an increase in nutrient availability through continental weathering intensification.

1   Introduction

The distribution of diatoms in the oceans is closely related to the cycling of carbon and silicon, and to the supply of nutrients:

15   nitrogen, phosphorus and iron are particularly important for diatoms, acting as limiting nutrients for phytoplankton proliferation (Hutchins and Bruland, 1998; Tyrrell, 1999). Within the biological pump, diatoms are responsible for a significant proportion of the export of organic carbon through photosynthesis. Their interactions with the silicon cycle also make them the main primary producer and exporter of organic silica in the oceans (Renaudie, 2016). They use dissolved silica (H_4SiO_4), supplied to the oceans by riverine input or recycled directly into the water column, to grow their siliceous frustules. In surface waters,

20   and particularly in conditions favourable for blooming, such as upwelling zones, diatoms are more likely to be grazed, while bacterial activity plays a major role in the dissolution of frustules in warm water areas, enhancing the recycling of dissolved

silica (Ragueneau et al., 2006). Another aspect of the biological pump is the gravitational sinking of diatoms in the water column, leading to the burial of diatom frustules in sediments. As a result, different types of sediments (e.g. diatom oozes, diatomites, cherts, etc.) are formed, depending on their diatom content (Zahajská et al., 2020).

25   In today's oceans, diatoms appear to be distributed mainly in nutrient-rich cold waters, such as in high latitude regions and upwelling zones (Tréguer et al., 2018). However, it is more difficult to reconstruct their geographic distribution in the past. The Palaeogene (66 to 23 million years ago [Ma]) was a period characterized by an initial warm climate, gradually cooling after the termination of the Early Eocene Climate Optimum (EECO; ~53 to ~49 Ma). Despite several studies examining temporal trends in early Cenozoic diatom-bearing sediments (Barron et al., 2015; Wade et al., 2020; Witkowski et al., 2021), temporal trends

30 in the global distribution of deep-sea diatom-bearing sediments in the Palaeogene remain sketchy. Bryłka et al. (2024) address how discussions on diatom involvement in biogeochemical cycling in the Palaeogene oceans tends to be based on very limited datasets. In addition, the mechanisms impacting diatom deposition during this period remain poorly understood. In shallow marine environments, Figus et al. (2024a) suggest the importance of climatic and tectonic controls on diatomite accumulation, with an influence of ocean circulation in open ocean settings from ~43.5 Ma. Furthermore, they indicate the presence of a

35 gap in diatomite deposition in epicontinental seas between ~46 and ~44 Ma, implying a contrasting pattern compared to the Atlantic, where biosiliceous fluxes peak between ~46 and ~42 Ma (Witkowski et al., 2021). Comparing these results raises a number of questions, including whether the Pacific and Indian oceans behaved similarly to the Atlantic during this period and, if not, why they reacted differently. Furthermore, is this apparent inverse relationship between the Atlantic and the shallow marine environments the result of a causal link, the influence of a common factor or an indirect correlation? To address these

40 questions, we present a global compilation of Palaeogene deep-sea diatom-bearing sediment occurrences, based on data reports from the Deep Sea Drilling Project (DSDP, 1966 to 1983), the Ocean Drilling Program (ODP, 1983 to 2003), the Integrated Ocean Drilling Program (IODP, 2003 to 2013) and the International Ocean Discovery Program (IODP, 2013 to 2024). Since 1966, over 400 expeditions have been carried out, enabling the collection of sediments from the Mesozoic to the present day, on nearly a global scale. The well-documented reports of these drilling campaigns provide a robust foundation for the creation

45 of our compilation, allowing its comparison with the dataset in Figus et al. (2024a) and various proxies. Based on this data analysis, we examine the importance of climate, tectonics and ocean circulation for the deposition of deep-sea diatom-bearing sediments during the Palaeogene.

2   Materials and methods

2.1   Lithology and terminology

50 Fossil marine diatoms are present in shallow and deep marine environments, where they can form (or be included in) different types of biogenic sediments. Mazzullo et al. (1988) denoted that the component of a sediment must represent at least 10% of its composition to be regarded as a modifier. Zahajská et al. (2020) propose the following classification: diatoms present in > 10% of a sediment can form a diatomaceous sediment (between 10 and 50% diatoms), a diatomaceous ooze (> 50%), a diatomaceous sedimentary rock (lithified diatomaceous sediment), or a diatomite (consolidated diatomaceous ooze). At this

55 stage, the silica contained in diatoms is known as opal-A (i.e., amorphous form). However, diagenetic processes, intensifying

with burial depth (and therefore with temperature and pressure), modify the structures of these sediments into shale (10 to

50% siliceous microfossils), porcelanite (20 to 85%) and chert (> 80%), where the opal-A becomes a silica polymorph called

opal-CT (Rice et al., 1995; Yanchilina et al., 2020). Since diagenesis modifies the structure of the sediment, determining the

biosiliceous origin of these rocks can be difficult, and the literature is often imprecise on the presence of diatoms, radiolarians

60 or sponge spicules in cherts (Witkowski et al., 2020). The final stage in diagenetic transformation of biosiliceous sediments is

the recrystallization of opal-CT (siliceous microfossils) into quartz (Zahajská et al., 2020). Whereas radiolarian 'ghosts' are

known to occasionally occur in such sediments (e. g., Gombos, 1984), diatoms are usually obliterated.

This compilation of deep-sea diatom-bearing sediments therefore covers all types of marine sediments containing as few as

traces of diatoms, up to lithologies composed mainly of diatoms, such as diatomites. Cherts have also been included if they are

65 documented as originating entirely or partially from diatoms.

2.2 Site selection

The compilation is based on DSDP, ODP and IODP reports. These international programmes are well documented, with

consistent reporting standards, and cover the world's oceans, with 1624 sites to date. No other type of drilling programme has

been added to the compilation, due to the lack of homogeneity of the published information.

70 This literature survey comprises 189 sites in the Arctic, Atlantic, Pacific, Indian and Southern oceans (see Figus et al., 2024b

and Fig. 1). Due to the difficulty of determining the palaeolatitude of the Southern Ocean, the high-latitude sites in the Southern

Hemisphere are divided by basins and included in the data for the Atlantic, Pacific and Indian Ocean.

Only sites considered to be deep-sea locations are selected, in order to investigate differences in diatom deposition mecha-

nisms between shallow shelf environments (Figus et al., 2024a) and deeper oceanic settings. The boundary between shallow

75 and deep marine environments is set here at a water depth of 200 metres. Hence, continental slopes are divided between

shallow (referred to as 'open ocean setting diatomites' in Figus et al., 2024a) and deep marine diatom-bearing sediments. Con-

sequently, DSDP, ODP and IODP sites where diatoms were deposited in shallow waters, such as sites 339, U1360 or U1567,

are not included in this study.

The second parameter limiting the compilation is the age of deposition. Only Palaeogene deposits (66 to 23 Ma) are included

80 in this compilation, binned into intervals with a 1 million-year (Myr) resolution. The ages are based on biostratigraphic studies

carried out by the drilling expeditions, using assemblages of nannofossils, foraminifera, diatoms, radiolarians or dinocysts

present in the sediments. All the ages in this study are given on the Gradstein et al. (2012) timescale.

Despite an overall good age determination, a few sites (notably of the older DSDP programme) were rejected due to insuffi-

cient age control (i.e., Sites 118, 267, 268, 270 and 674) reported in the literature.

85 The sites palaeolatitudes in each time bin (see Fig. 2e) were computed with GPlates (Müller et al., 2018) using the Torsvik

et al. (2019) rotation model. The sites palaeobathymetry in each time bin (see Fig. 2c) was then calculated by extracting

the depth from Straume et al. (2024) palaeotopographic maps at the palaeocoordinates computed above. Given those maps

resolution and the uncertainty of their underlying model, the reported palaeodepths are thus a somewhat broad estimate of the bathymetry near the sites.

2.3 Sampling normalization

In order to provide a baseline for the geographic distribution of the diatom-bearing sediments, we have also compiled a list of all the DSDP, ODP and IODP deep-sea sites containing Palaeogene sediments, regardless of their lithology. To do so, we use the site age profiles, as compiled in the National Geophysical Data Center for DSDP Legs 1 to 96 and ODP Legs 101 to 129 (National Geophysical Data Center, 2000, 2001), in the Janus database for ODP Legs 178 to 201 (Mithal and Becker, 2006)), and as reported in the Preliminary Results of ODP Legs 130 to 177 and IODP Expeditions 301 to 402. The ages provided by those various sources are limited in resolution, as they are provided in the form of Epoch/Stage names rather than a numerical age. The resulting dataset can be found in Supplementary material.

This baseline is also used to normalize the number of diatom-bearing sites seen in the deep-sea: a classical rarefaction (Sanders, 1968) is applied to the number of sites drilled during each time bin (with a quota of 90 sites), and to the number of sites drilled per basin (with a quota of 25 sites) during each time bin, over 10 000 trials. Fig. 3 shows the median number of diatom-bearing sites over each trial, as well as its interquartile range.

2.4 Comparisons with radiolarians

Finally, to provide contrast to the diatom dataset and to allow us to understand any discrepancy between our collection of diatom-related cherts and the timeseries of chert occurrences reported in Muttoni and Kent (2007; Fig. 2), we updated the dataset of radiolarian abundances reported in Renaudie (2016), based on smear slide descriptions from DSDP Legs 1 to 96, ODP Legs 101 to 129, 178 to 201 and IODP Expeditions 206 to 308, by adding sites for which new age models were available in the Neptune Database (Renaudie et al., 2023).

3 Results and interpretation

3.1 Impact of biases on the observed pattern

In order to be able to draw comparisons with environmental parameters, it is first necessary to consider potential biases in the deep-sea diatom-bearing sediment data.

3.1.1 Sediments preservation

As discussed in section 2.1, diagenetic factors are very likely to introduce an inherent bias into our compilation. Consequently, even though we have considered all the concentrations of diatoms in the sediments in our compilation, including traces, the possibility of a bias arises. If diatoms were undetectable in the cherts drilled and analyzed by the shipboard scientists during the drilling expeditions, and thus not included in their reports, these cherts would not have been included in our compilation

(see section 2 Material and methods for further explanation on site selection). In order to verify this option, a distinction is made between cherts and other sediments in each ocean (except the Arctic, for which no chert occurrence records were found). These results are compared with those of Muttoni and Kent (2007) in Fig. 1. From the middle Eocene onwards, our results are similar, but those from the Palaeocene and early Eocene differ. Considering that Muttoni and Kent (2007) include all types of cherts, while our compilation is based on diatoms only, two hypotheses can be put forward: 1) some sites are absent from our compilation due to the impossibility of distinguishing diatoms and radiolarians in the cherts, or 2) in the Palaeocene-early Eocene, most cherts were derived from radiolarian skeletons. The answer remains indeterminable, owing to the dissolution of siliceous microfossils, and the presence only of preserved radiolarians in a chert does not exclude the likelihood that originally, diatoms may also have been present. Diatoms are dissolved more easily than radiolarians, as they are less heavily silicified, due to their size and surface/volume ratio. This difference affects the time it takes for the particles to sink (Stoke's law). Particles that sink slowly and have a higher surface ratio, have a greater reaction potential.

3.1.2 Sampling bias

The various deep-sea drilling campaigns did not recover sediments of all ages at an equal rate: in particular, the early Palaeogene (early Palaeocene to early Eocene) was significantly undersampled compared to the subsequent stages (see Fig. 1). Correcting for this bias using rarefaction, we show that while most of the time series pattern in each basin, as well as globally, remain mostly unchanged and consistent from the end of the Early Eocene onwards, the previous time interval does show significant changes, namely rather than a steep, uniform increase in the number of diatom-bearing sites from the K/Pg boundary to the middle Eocene. What we actually see is that in the middle Palaeocene, diatom-bearing sites are as frequent (proportionally) as they are in the middle to late Eocene, while the late Palaeocene shows an abrupt drop, recovering only at the end of the Ypresian. Whether this early Eocene diatom gap (particularly clear in the Atlantic) is real, or a preservation effect (as it is coeval with a known chertification event in the North Atlantic; e. g., Muttoni and Kent, 2007) remains unclear, though as was shown above, those cherts are potentially not diatom-related, but radiolarian-related.

3.2 Impact of nutrients and ocean circulation

Figure 4 presents several geochemical proxies potentially influencing diatom distribution. Chemical ratios like $^{87}Sr/^{86}Sr$ and δ^7Li (strontium and lithium isotopes, respectively) track the degradation of continental rocks by interaction with CO_2 and water, combined to form carbonic acid (H_2CO_3). This reaction consumes atmospheric CO_2 and releases the anions and cations present in the weathered rock, such as dissolved silica (H_4SiO_4; Froelich and Misra, 2014) or phosphorus (P; Föllmi, 1995). Records of pCO_2 (Fig. 2a) and silicate weathering are therefore closely related, as are phosphorus and deep-sea diatom-bearing sediments (Fig. 4d, e). Bioavailable nitrogen, however, is mainly supplied to the oceans by organisms (e.g. cyanobacteria) capable of capturing dinitrogen (N_2) from the atmosphere or their environment, and fixing it into ammonium (NH_4+), then nitrite (NO_2-) and nitrate (NO_3-) by nitrification (Kast et al., 2019). With the exception of N_2, these other forms of nitrogen, as well as phosphorus, can be used by phytoplankton and be recycled in the oceans during the degradation or grazing of living diatoms and other organisms (Tyrrell, 1999).

3.2.1 Early Palaeogene

After the Cretaceous-Palaeogene boundary, the decrease in silicate weathering proxy values in the Palaeocene (Fig. 4) is linked to the prevalence of peneplain landforms (Misra and Froelich, 2012; Froelich and Misra, 2014; Tsekhovsky, 2015). Misra and Froelich (2012) propose two possibilities to interpret the lower δ^7Li values in the late Palaeocene–early Eocene: 1) the input of light Li from rivers to the oceans, in association with the numerous hyperthermal events leading to intensified weathering of cation-depleted peneplain rocks at low latitudes; or 2) the influence of Large Igneous Provinces (LIPs) such as the Deccan Traps or the North Atlantic Igneous Province (NAIP). As basalt is rapidly weathered yielding lighter Li, the position of India with freshly erupted LIPs at the Equator around the Palaeocene-Eocene boundary might have led to the drop in δ^7Li at this period. A similar process may have occurred with the NAIP during the Middle Eocene Climatic Optimum (MECO; ~40.5 to ~40 Ma), leading to a reduction in the number of diatom-bearing sediments in the North Atlantic (Fig. 4e). Furthermore, this second possibility may explain the two drops in ^{87}Sr/^{86}Sr at the EECO and MECO, and would be consistent with the hypothesis of McArthur et al. (2001), supporting the idea of a decrease in ^{87}Sr/^{86}Sr linked to the LIPs in the Palaeocene. The phosphorus record (Fig. 4d), which is indicative of continental weathering rates, is also more consistent with this scenario. The P_{tot} curve represents all forms of phosphate, while P_{bio} is a measure of bioavailable phosphorus. Föllmi (1995) explains that the similarity between the two curves indicates that changes in bioavailable phosphorus, originating from chemical weathering, are similar to the total continental weathering. Therefore, although δ^7Li and ^{87}Sr/^{86}Sr are lower in the early Palaeogene, the high accumulation rates of phosphorus are consistent with enhanced continental weathering driven by hyperthermal events (Penman, 2016).

Comparison of the δ^7Li record with the number of deep-sea diatom-bearing sediments (this study) and the number of shallow marine diatomite occurrences (Figus et al., 2024a) suggests that diatoms were mainly accumulating in the North Atlantic and Eurasian epicontinental basins (in particular the western Siberian marine areas) during the early Palaeogene (Fig. 1), whereas the low and mid-latitudes of the Southern Hemisphere appear to be depleted in this respect (Fig. 5a). Moreover, the number of epicontinental sea diatomite occurrences (Fig. 1) is very similar to P_{bio} (Fig. 4d), demonstrating the influence of nutrients – provided here by continental weathering during hyperthermal events – on diatom deposition. However, despite an increase in the number of diatom-bearing deposits in the Atlantic during the early Palaeogene, none of the deep-sea diatom-bearing records appear to be correlated with phosphorus availability. After correcting for sampling bias (Fig. 3), it appears that early-middle Palaeocene diatom-bearing sediments are probably artificially low, due to the number of drilled sediments dating from this age. Thus, the apparent trend of steady increase from the Cretaceous-Palaeogene boundary is most likely false, but the amount of diatom-bearing sediments show a substantial increase from 48 Ma onwards.

Differences between shallow and deep-sea realms might be explained by ocean circulation. Although nutrients can be easily distributed by rivers in near-shore environments, the influence of transport remains limited (Araujo et al., 2017; Katz et al., 2020). Phytoplankton would therefore bloom mainly near coastal areas and in shallow basins. In the Palaeocene, δ^{15}N, which represents the ratio of denitrification (i.e., reduction of nitrate to dinitrogen by oxidation of organic matter) of ^{15}N/^{14}N, was particularly high in the Pacific before falling abruptly around the PETM onset (Fig. 4c). According to Kast et al. (2019), elevated

δ^{15}N indicates suboxic conditions, presumably due to increased stratification of the oceans during this period. A comparison

185 with the number of diatom-bearing sites in the Pacific suggests an inverse relationship between these two records, which would be consistent with the effect of global ocean ventilation on nutrient distribution and diatom deposition. This hypothesis could also apply to the Indian and Atlantic oceans. While diatom-bearing sediments in the Atlantic are distributed near the margins that provided nutrients in the Palaeocene, the subsidence of the Greenland–Scotland Ridge may have improved ocean ventilation from the Eocene onwards (Vahlenkamp et al., 2018), and allowed the formation of intermediate waters in the North

190 Atlantic around Greenland.

3.2.2 Middle Eocene diatomite gap

In Figs 4 and 2, a peak in continental weathering and temperature proxies is observed, as well as a drop in pCO$_2$, at about the same time as the decrease in the Atlantic diatom-bearing sediment occurrence record, from ~42.5 Ma onwards. These results suggest that global temperatures have increased, and that continental weathering has intensified. In addition, the lowering

195 of δ^{15}N (Fig. 4c) is caused by the remineralization of organic nitrogen into nitrate, linked to the preferential uptake of 14N by phytoplankton (Auderset, 2020). Moore (2008) suggests that nutrient and dissolved silica recycling rates may have been intensified by an increase in the metabolic rates of marine organisms, linked to the warm temperatures of the early Eocene (Olivarez Lyle and Lyle, 2006). With the increased weathering and recycling of N in the Lutetian, nutrients were highly available for diatoms during the diatomite gap, but differences in the distribution of P and N influenced the diatom-bearing sediments

200 accumulation. P is distributed predominantly at the margins (e.g. North Atlantic and Northern Indian Ocean), reflecting its weathering-related origin, whereas bioavailable N is supplied by upwelling as in the Central and Equatorial Pacific. Figure 1 compares data obtained in this study with the shallow marine diatomite records of Figus et al. (2024a) and suggests contrasting patterns in diatom deposition between the North Atlantic – as shown in Fig. 2d-e, these deposits are mainly distributed in the North Atlantic – and epicontinental seas during the middle Eocene. In the Pacific and Indian oceans, the number of deep-sea

205 diatom-bearing sediment occurrences increases from the end of the EECO and through the diatomite gap, while the number of diatomite occurrences decreases in epicontinental seas (Fig. 1). In the Pacific, the curve marks a step during the diatomite gap, before abruptly increasing again at the same time as the number of shallow marine diatomite occurrences. Global cooling following the EECO may be responsible for the general increase in the number of diatom-bearing sites in the Pacific, but the sampling bias shown in Fig. 3 suggests that the number of diatom-bearing sites in the Pacific increases with the number of

210 drilled sites in the early to middle Eocene. However, it seems that the peak in diatom-bearing sediment occurrences in the Indian Ocean during the middle Eocene is genuine, like in the Atlantic (Fig. 13). In addition to biosiliceous production, diatom diversity (Fig. 1) is increasing (Lazarus et al., 2014). Sims et al. (2006) and Witkowski (2022) have already reported this explosion in diversity, explaining that numerous genera have appeared, in particular monospecific ones. Figus and Witkowski (2024), for example, describe two monospecific genera from the middle Eocene, discovered in samples from the North Atlantic, which

215 coincide with the peak in diversity and the number of Atlantic diatom-bearing sediments.

Figus et al. (2024a) attribute the diatomite gap between ~46 and ~44 Ma to tectonic reorganization, involving, for example, the closure of the western Siberian Sea strait and the Arctic basin connection, which probably led to the establishment of more

terrigenous-dominated sedimentation (Akhmetiev et al., 2010). Inter-basin reorganization of the area may have been respon-
sible for the increase in continental weathering, resulting in lower $p\text{CO}_2$ and enhanced phosphorus inputs. Witkowski et al.
220 (2021) suggest that the Northern Component Water may have improved Atlantic ocean circulation in the middle Eocene, en-
abling a better distribution of nutrients, and thus intensifying biosiliceous production. It could be hypothesized that biosiliceous
production may have also contributed to the decrease in $p\text{CO}_2$, but the resolution of our dataset is too coarse to provide an
answer.

3.2.3   Latitudinal and inter-basin shifts in the distribution of diatom-bearing sediments

225 A close examination of the occurrences of shallow marine diatomite deposited in open ocean conditions (Fig. 1) suggests
a similar pattern within the Pacific and Indian Ocean curves, although the number of shallow marine diatomite occurrences
appears to increase as the number of deep-sea diatom-bearing sediment occurrences decreases, and inversely, from the Priabo-
nian onwards. Interestingly, almost all the diatomite occurrences in open ocean settings in Figus et al. (2024a) are distributed
around the Pacific (i. e. Kamchatka and the west coasts of North and South America), starting with a high number of diatomite
230 occurrences along the west coast of North America in the Bartonian, followed by increased accumulation of diatomite on the
western continental slope of South America in the Priabonian, before the onset of the deposition of shallow marine diatomite
in the Kamchatka region in the Oligocene.

Despite the general picture of a sluggish Eocene ocean (Haq, 1981; Keller, 1983; Barron, 1987; Miller, 1992; Huber and
Sloan, 2001), Moore (2008) suggests that there is no evidence of weaker Eocene thermohaline circulation, and that only wind-
235 induced ocean currents have been slowed. Consequently, the increase in the number of deep-sea diatom-bearing sediment
occurrences, and later shallow marine diatomites, in the Pacific and Indian oceans, may be the reflection of improved ocean
ventilation. Moore et al. (2008) present results on the recovery of Eocene radiolarian zones in several basins, which display a
similar pattern to our results on the number of diatom-bearing sediments (Fig. 1), showing an apparent shift from the Atlantic
to the Pacific and Indian basins in the late Eocene. This change in the distribution of siliceous microfossils around 43 Ma is
240 interpreted as the result of a shift in the formation of deep ocean waters, from the North Pacific to the Southern Ocean (Thomas,
2004; Moore et al., 2008). Furthermore, Fig. 5 shows that around the same time, the distribution of the diatom-bearing (Fig.
5a) and radiolarian (Fig. 5b) deposits changed from mid-northern to tropical latitudes.

It has long been a widely repeated statement that as the ocean cooled through the Palaeogene, the Southern Ocean progres-
sively became the key diatom accumulation locus. This perspective seems to have been formulated in the early days of the
245 DSDP era (e. g., Fenner, 1984, 1995), which shaped our overall understanding of diatom-bearing deposit distribution in deep
time. Bryłka et al. (2024) challenged such views, and showed that there was very little quantitative support for whatever overall
statements on how diatoms may have reacted to the rapid cooling at the Eocene-Oligocene Transition (EOT; ~33.9 Ma). While
the present study also does not provide a quantitative perspective on diatom accumulation, our data may be interpreted as a
measure of geographic distribution of diatom preservation in sediments, with an underlying caveat that seafloor preservation
250 reflects the surface water production rates.

Figure 2d-e shows cumulative plots of the distribution of diatom-bearing sites through time by latitude and by ocean basin. These indicate that through our entire study interval, the tropics and mid-northern latitudes have consistently witnessed the most widespread deposition of diatom-bearing sediments (Fig. 4e). The contribution of northern high latitude and mid-southern latitude zones is negligible, but the distribution of drilling sites in the Atlantic Ocean shows a substantial bias against the

255   Southern Hemisphere (Witkowski et al., 2020), and so this perspective may be inaccurate. The southern high-latitude belt shows higher percentages in the Palaeocene, when diatom-bearing sediments are generally sparse (thus making a biased view more likely), and in the late Eocene-Oligocene interval (Fig. 2e). In the latter case, however, the increase takes place not at the Eocene-Oligocene boundary, but at the onset of the late Eocene (~37.5 Ma).

When viewed by ocean basin, we note that through the Palaeocene and early Eocene (except for a brief early Palaeocene

260   interval of increased Pacific contribution), diatom deposition is largely focused in the Atlantic Ocean, consistent with the observations summarized above and in previous studies (e. g., Witkowski et al., 2020) (Fig. 2d). From around the Palaeocene-Eocene boundary, and especially so from the termination of the EECO at ~49 Ma, the Indian Ocean and the Pacific show a progressively higher proportion of diatom-bearing sites relative to the Atlantic. These proportions largely stabilize at ~41 Ma and remain so, with subordinate fluctuations, until the end of the Palaeogene. Notably, there is no drastic inter-basinal shift at

265   the Eocene-Oligocene Transition. Thus, again, if our data are to be treated as a measure of geographic extent of biosiliceous production, the pattern of diatom-bearing site distribution largely opposes the traditional view of biogenic silica accumulation being progressively more focused in the Southern Ocean in the latter half of the Palaeogene.

3.3   Impact of glacial events and Antarctic Ice Sheet setting

A peak in the number of diatom-bearing sites occurs at ~37.5 Ma in the Pacific and Indian oceans (Fig. 1). Fontorbe et al.

270   (2017) describe an enrichment of Pacific equatorial waters in dissolved silica from 37 Ma, in relation to the widening of the Drake Passage and the deepening of the Tasman gateway, affecting ocean circulation. However, Pascher et al. (2015) report the response of radiolarians to a glacial event in the Pacific: the Priabonian Oxygen Isotope Maximum (PrOM; ~37.3 Ma). This event is associated with a positive oxygen isotope excursion and a continental-scale glaciation of Antarctica (Van Breedam et al., 2022). This early ice sheet expansion might have enhanced continental weathering, contributing to phosphorus (Fig. 4d)

275   and dissolved silica enrichments (Hawkings et al., 2017) that led to increases in the abundance, preservation and diversity of radiolarians (Pascher et al., 2015) and diatoms (Fig. 1).

Similarly, the number of diatom-bearing sediment occurrences in the Pacific and Indian oceans, as well as diatom diversity (Fig. 1), appear to respond to the Oligocene glacial events Oi-1 (~33.6 Ma; Pälike et al., 2006) and Oi-1a (~32.8 Ma; Galeotti et al., 2016), which mark the onset of a permanent Antarctic Ice Sheet. The perturbations of the climate and Antarctic Ice Sheet

280   are closely related, with retreats of the ice sheet during warmer periods, and its expansion during cooler periods (Zachos et al., 2001) such as the global cooling set at the Eocene-Oligocene Transition. The fact that the number of deep-sea diatom-bearing occurrences in the Pacific and Indian oceans does not peak at exactly the same time (first the Indian Ocean with Oi-1, then the Pacific with Oi-1a) might be a problem with the resolution of our data, or may be related to a basin-to-basin fractionation of deep-sea biogenic sediments. Witkowski et al. (2021) reported several shifts in biogenic silica fluxes between the Pacific and

285 Atlantic, around 42, 37 and 35 Ma. These shifts are all illustrated in Fig. 1, and the decoupling between the Pacific and the Atlantic may be explained by the fractionation of biogenic sediments by deep ocean circulation (Berger, 1970; Witkowski et al., 2021), as explained in section 3.2.3. Another peak in the number of deep-sea diatom-bearing sediment occurrences is observed in each basin after the Oi-2 (~30.35 Ma; Wade and Pälike, 2004), another Oligocene glacial event. Due to the differences of resolution between the dating of these climatic events and our results, the cause of the increased number of diatom-bearing

290 deposits remains uncertain, but the presence of a permanent Antarctic Ice Sheet impacting continental weathering and nutrient distribution during this period appears to be a plausible explanation.

3.4 Arctic Ocean

Only four of the sites drilled by ODP and IODP in the Arctic Ocean contain Palaeogene diatom-bearing sediments. As a result, the data are not representative enough of the Arctic basin to be interpreted in this study. Nevertheless, these sites

295 have been retained in the compilation to ensure the global representation of deep-sea diatom-bearing sediment distribution. Figure 1 illustrates that diatom-bearing sediments started accumulating at our Arctic sites during the EECO, which could be interpreted as an effect of global cooling (Fig. 2b). Additionally, the Arctic curve indicates a slight increase in the number of diatom-bearing sediments during the diatomite gap, simultaneously with the step marked by the Pacific curve, and during the Oi-2 glacial event. Ocean circulation, and indirectly climate, might therefore explain these peaks, as in the other oceans. This

300 remains, however, a hypothesis, and it would be necessary to study a larger number of diatom-bearing sites in the Arctic to formulate an interpretation.

4 Conclusion

Despite the high number of drilling expeditions which covered the world's oceans, compiling deep-sea diatom-bearing data is challenging, due to the unequal temporal and spatial coverage of the sediments. In addition, the diagenetic processes occurring

305 with increasing burial depths impact the preservation of siliceous microfossils, making their identification more difficult in the oldest sediments. However, the present study suggests that the number and distribution of deep-sea diatom-bearing sediments is mainly controlled by the nutrient availibility and ocean circulation. Climate appears to have only an indirect correlation with our results, which may be linked with the extension of the Antarctic Ice Sheet during the Oligocene global cooling.

The comparison of these results with shallow marine diatomites suggests that the increase in the number of deep-sea diatom-

310 bearing sediment occurrences (particularly in the Atlantic) during the diatomite gap (~46 to ~44 Ma; Figus et al., 2024a) is probably related to the tectonic reorganizations occurring during this period. These palaeogeographic changes caused the cessation of shallow marine diatomite deposition, and an increase in nutrient availability through continental weathering intensification.

Data availability. The compilations of deep-sea diatom-bearing sediments, radiolarian occurrences and age profiles can be found on Zenodo
315 (Figus et al., 2024b). Palaeogeographic maps showing all drilled sites in each 1 Myr time bin can be found in the Supplementary Materials.

Author contributions. JW designed the study. CF and JW prepared the compilation. JR processed the data. All co-authors participated in the
interpretation of the data. CF prepared the manuscript, with contributions from all co-authors.

Competing interests. The authors declare that they have no conflict of interest.

References

320 Akhmetiev, M. A., Zaporozhets, N. I., Iakovleva, A. I., Aleksandrova, G. N., Beniamovsky, V. N., Oreshkina, T. V., Gnibidenko, Z. N., and Dolya, Z. A.: Comparative analysis of marine paleogene sections and biota from West Siberia and the Arctic Region, Stratigr. Geol. Correl., 18, 635–659, https://doi.org/10.1134/S0869593810060043, 2010.

Araujo, M., Noriega, C., Hounsou-gbo, G. A., Veleda, D., Araujo, J., Bruto, L., Feitosa, F., Flores-Montes, M., Lefèvre, N., Melo, P., Otsuka, A., Travassos, K., Schwamborn, R., and Neumann-Leitão, S.: A Synoptic Assessment of the Amazon River-
325 Ocean Continuum during Boreal Autumn: From Physics to Plankton Communities and Carbon Flux, Front. Microbiol., 8, 1358, https://doi.org/10.3389/fmicb.2017.01358, 2017.

Auderset, A.: Nutrient cycling in the oligotrophic ocean over the past 65 million years, 2020.

Barron, E. J.: Eocene equator-to-pole surface ocean temperatures: A significant climate problem?, Paleoceanography, 2, 729–739, https://doi.org/10.1029/PA002i006p00729, 1987.

330 Barron, J. A., Stickley, C. E., and Bukry, D.: Paleoceanographic, and paleoclimatic constraints on the global Eocene diatom and silicoflagellate record, Palaeogeogr. Palaeoclimatol. Palaeoecol., 422, 85–100, https://doi.org/10.1016/j.palaeo.2015.01.015, 2015.

Berger, W. H.: Biogenous Deep-Sea Sediments: Fractionation by Deep-Sea Circulation, Geol Soc America Bull, 81, 1385, https://doi.org/10.1130/0016-7606(1970)81[1385:BDSFBD]2.0.CO;2, 1970.

Bryłka, K., Witkowski, J., and Bohaty, S. M.: Biogenic silica accumulation and diatom assemblage variations through the Eocene-
335 Oligocene Transition: A Southern Indian Ocean versus South Atlantic perspective, Palaeogeogr. Palaeoclimatol. Palaeoecol., 636, 111 971, https://doi.org/10.1016/j.palaeo.2023.111971, 2024.

Fenner, J.: Eocene-Oligocene Planktic Diatom Stratigraphy in the Low Latitudes and the High Southern Latitudes, Micropaleontology, 30, 319, https://doi.org/10.2307/1485708, 1984.

Fenner, J.: Late Cretaceous to Oligocene planktic diatoms, in: Plankton Stratigraphy, edited by Bolli, H., Saunders, J., and Perch-Nielsen,
340 K., vol. 2, p. 1006, Cambridge Univ. Press, 1995.

Figus, C. and Witkowski, J.: New taxa of the Rhaphoneidaceae Forti (Bacillariophyta) from the middle Eocene, Diatom Research, 39, 1–11, https://doi.org/10.1080/0269249X.2024.2319356, 2024.

Figus, C., Bialik, O. M., Gladenkov, A. Y., Oreshkina, T. V., Renaudie, J., Smirnov, P., and Witkowski, J.: Climatic and tectonic controls on shallow-marine and freshwater diatomite deposition throughout the Palaeogene, Clim. Past, 20, 2629–2644, https://doi.org/10.5194/cp-
345 20-2629-2024, 2024a.

Figus, C., Renaudie, J., Bialik, O. M., and Witkowski, J.: Compilations of Palaeogene deep-sea diatom-bearing sediments and associated data, https://doi.org/10.5281/ZENODO.14245396, 2024b.

Föllmi, K.: 160 m.y. record of marine sedimentary phosphorus burial: Coupling of climate and continental weathering under greenhouse and icehouse conditions, 23, 503–506, 1995.

350 Fontorbe, G., Frings, P. J., De La Rocha, C. L., Hendry, K. R., Carstensen, J., and Conley, D. J.: Enrichment of dissolved silica in the deep equatorial Pacific during the Eocene-Oligocene, Paleoceanography, 32, 848–863, https://doi.org/10.1002/2017PA003090, 2017.

Foster, G. L., Royer, D. L., and Lunt, D. J.: Future climate forcing potentially without precedent in the last 420 million years, Nat Commun, 8, 14 845, https://doi.org/10.1038/ncomms14845, 2017.

Froelich, F. and Misra, S.: Was the Late Paleocene-Early Eocene Hot Because Earth Was Flat? An Ocean Lithium Iso-355 tope View of Mountain Building, Continental Weathering, Carbon Dioxide, and Earth's Cenozoic Clima, oceanog, 27, 36–49, https://doi.org/10.5670/oceanog.2014.06, 2014.

Galeotti, S., DeConto, R., Naish, T., Stocchi, P., Florindo, F., Pagani, M., Barrett, P., Bohaty, S. M., Lanci, L., Pollard, D., Sandroni, S., Talarico, F. M., and Zachos, J. C.: Antarctic Ice Sheet variability across the Eocene-Oligocene boundary climate transition, Science, 352, 76–80, https://doi.org/10.1126/science.aab0669, 2016.

360 Gombos, A.: Late Paleocene diatoms in the Cape basin, vol. 73 of *Initial Reports of the Deep Sea Drilling Project*, U.S. Government Printing Office, https://doi.org/10.2973/dsdp.proc.73.1984, 1984.

Gradstein, F. M., Ogg, J. G., Schmitz, M., and Ogg, G.: The Geologic Time Scale 2012 2-Volume Set, Elsevier Science, ISBN 978-0-444-59448-8, OCLC: 956664433, 2012.

Haq, B. U.: Paleogene Paleoceanography : Early Cenozoic Oceans Revisited., pp. 71–81, 1981.

365 Hawkings, J. R., Wadham, J. L., Benning, L. G., Hendry, K. R., Tranter, M., Tedstone, A., Nienow, P., and Raiswell, R.: Ice sheets as a missing source of silica to the polar oceans, Nat Commun, 8, 14 198, https://doi.org/10.1038/ncomms14198, 2017.

Huber, M. and Sloan, L. C.: Heat transport, deep waters, and thermal gradients: Coupled simulation of an Eocene greenhouse climate, Geophys. Res. Lett., 28, 3481–3484, https://doi.org/10.1029/2001GL012943, 2001.

Hutchins, D. A. and Bruland, K. W.: Iron-limited diatom growth and Si:N uptake ratios in a coastal upwelling regime, Nature, 393, 561–564, 370 https://doi.org/10.1038/31203, 1998.

Kast, E. R., Stolper, D. A., Auderset, A., Higgins, J. A., Ren, H., Wang, X. T., Martínez-García, A., Haug, G. H., and Sigman, D. M.: Nitrogen isotope evidence for expanded ocean suboxia in the early Cenozoic, https://doi.org/10.1126/science.aau5784, 2019.

Katz, T., Weinstein, Y., Alkalay, R., Biton, E., Toledo, Y., Lazar, A., Zlatkin, O., Soffer, R., Rahav, E., Sisma-Ventura, G., Bar, T., Ozer, T., Gildor, H., Almogi-Labin, A., Kanari, M., Berman-Frank, I., and Herut, B.: The first deep-sea mooring station in the eastern Levantine 375 basin (DeepLev), outline and insights into regional sedimentological processes, https://doi.org/10.1016/j.dsr2.2019.104663, 2020.

Keller, G.: Paleoclimatic analyses of middle Eocene through Oligocene planktic foraminiferal faunas, https://doi.org/10.1016/0031-0182(83)90049-4, 1983.

Lazarus, D., Barron, J., Renaudie, J., Diver, P., and Türke, A.: Cenozoic Planktonic Marine Diatom Diversity and Correlation to Climate Change, PLoS ONE, 9, e84 857, https://doi.org/10.1371/journal.pone.0084857, 2014.

380 Mazzullo, J., Meyer, A., and Kidd, R.: New sediment classification scheme for the Ocean Drilling Program, in: Handbook for Ship-board Sedimentologists, edited by Mazzullo, J. and Graham, A., no. 8 in Ocean Drilling Program Technical Notes, pp. 45–67, https://doi.org/10.2973/odp.tn.8.1988, 1988.

McArthur, J. M., Howarth, R. J., and Bailey, T. R.: Strontium Isotope Stratigraphy: LOWESS Version 3: Best Fit to the Marine Sr-Isotope Curve for 0–509 Ma and Accompanying Look-up Table for Deriving Numerical Age, The Journal of Geology, 109, 155–170, 385 https://doi.org/10.1086/319243, 2001.

McGill, R., Tukey, J., and Larsen, W.: Variations of box plots, pp. 12–16, 1978.

Miller, K. G.: 8. Middle Eocene to Oligocene Stable Isotopes, Climate, and Deep-Water History: The Terminal Eocene Event?, in: Eocene-Oligocene Climatic and Biotic Evolution, edited by Prothero, D. R. and Berggren, W. A., pp. 160–177, Princeton University Press, ISBN 978-1-4008-6292-4, https://doi.org/10.1515/9781400862924.160, 1992.

390 Misra, S. and Froelich, P. N.: Lithium Isotope History of Cenozoic Seawater: Changes in Silicate Weathering and Reverse Weathering, Science, 335, 818–823, https://doi.org/10.1126/science.1214697, 2012.

Mithal, R. and Becker, D. G.: The Janus database: providing worldwide access to ODP and IODP data, SP, 267, 253–259, https://doi.org/10.1144/GSL.SP.2006.267.01.19, 2006.

Moore, T.: Chert in the Pacific: Biogenic silica and hydrothermal circulation, Palaeogeogr. Palaeoclimatol. Palaeoecol., 261, 87–99, https://doi.org/10.1016/j.palaeo.2008.01.009, 2008.

Moore, T. C., Jarrard, R. D., Olivarez Lyle, A., and Lyle, M.: Eocene biogenic silica accumulation rates at the Pacific equatorial divergence zone, Paleoceanography, 23, 2007PA001 514, https://doi.org/10.1029/2007PA001514, 2008.

Müller, R. D., Cannon, J., Qin, X., Watson, R. J., Gurnis, M., Williams, S., Pfaffelmoser, T., Seton, M., Russell, S. H. J., and Zahirovic, S.: GPlates: Building a Virtual Earth Through Deep Time, Geochem Geophys Geosyst, 19, 2243–2261, https://doi.org/10.1029/2018GC007584, 2018.

Muttoni, G. and Kent, D. V.: Widespread formation of cherts during the early Eocene climate optimum, Palaeogeogr. Palaeoclimatol. Palaeoecol., 253, 348–362, https://doi.org/10.1016/j.palaeo.2007.06.008, 2007.

National Geophysical Data Center: Core Data from the Deep Sea Drilling Project Legs 1–96, World Data Center for Marine Geology & Geophysics, Seafloor Series, 1, http://www.ngdc.noaa.gov/mgg/fliers/00mgg03.html, 2000.

National Geophysical Data Center: Core Data from the Deep Sea Drilling Project Legs 101–129. World Data Center for Marine Geology & Geophysics, Seafloor Series, 2, http://www.ngdc.noaa.gov/mgg/geology/odp/start.html, 2001.

Olivarez Lyle, A. and Lyle, M. W.: Missing organic carbon in Eocene marine sediments: Is metabolism the biological feedback that maintains end-member climates?, Paleoceanography, 21, 2005PA001 230, https://doi.org/10.1029/2005PA001230, 2006.

Pälike, H., Norris, R. D., Herrle, J. O., Wilson, P. A., Coxall, H. K., Lear, C. H., Shackleton, N. J., Tripati, A. K., and Wade, B. S.: The Heartbeat of the Oligocene Climate System, Science, 314, 1894–1898, https://doi.org/10.1126/science.1133822, 2006.

Pascher, K. M., Hollis, C. J., Bohaty, S. M., Cortese, G., McKay, R. M., Seebeck, H., Suzuki, N., and Chiba, K.: Expansion and diversification of high-latitude radiolarian assemblages in the late Eocene linked to a cooling event in the southwest Pacific, Clim. Past, 11, 1599–1620, https://doi.org/10.5194/cp-11-1599-2015, 2015.

Penman, D. E.: Silicate weathering and North Atlantic silica burial during the Paleocene-Eocene Thermal Maximum, Geology, 44, 731–734, https://doi.org/10.1130/G37704.1, 2016.

Ragueneau, O., Schultes, S., Bidle, K., Claquin, P., and Moriceau, B.: Si and C interactions in the world ocean: Importance of ecological processes and implications for the role of diatoms in the biological pump, Global Biogeochemical Cycles, 20, 2006GB002 688, https://doi.org/10.1029/2006GB002688, 2006.

Renaudie, J.: Quantifying the Cenozoic marine diatom deposition history: links to the C and Si cycles, Biogeosciences, 13, 6003–6014, https://doi.org/10.5194/bg-13-6003-2016, 2016.

Renaudie, J., Lazarus, D., and Diver, P.: Archive of Neptune (NSB) database backups, https://doi.org/10.5281/ZENODO.10063218, 2023.

Rice, S., Freund, H., Huang, W., Clouse, J., and Isaacs, C.: Application of Fourier Transform Infrared Spectroscopy to Silica Diagenesis: The Opal-A to Opal-Ct Transformation, SEPM JSR, Vol. 65A, 639–647, https://doi.org/10.1306/D4268185-2B26-11D7-8648000102C1865D, 1995.

Sanders, H.: Marine benthic diversity: a comparative study, pp. 243–282, 1968.

Sims, P. A., Mann, D. G., and Medlin, L. K.: Evolution of the diatoms: insights from fossil, biological and molecular data, Phycologia, 45, 361–402, https://doi.org/10.2216/05-22.1, 2006.

Straume, E. O., Steinberger, B., Becker, T. W., and Faccenna, C.: Impact of mantle convection and dynamic topography on the Cenozoic paleogeography of Central Eurasia and the West Siberian Seaway, Earth and Planetary Science Letters, 630, 118 615, https://doi.org/10.1016/j.epsl.2024.118615, 2024.

Thomas, D. J.: Evidence for deep-water production in the North Pacific Ocean during the early Cenozoic warm interval, Nature, 430, 65–68, https://doi.org/10.1038/nature02639, 2004.

Torsvik, T. H., Steinberger, B., Shephard, G. E., Doubrovine, P. V., Gaina, C., Domeier, M., Conrad, C. P., and Sager, W. W.: Pacific-Panthalassic Reconstructions: Overview, Errata and the Way Forward, Geochem Geophys Geosyst, 20, 3659–3689, https://doi.org/10.1029/2019GC008402, 2019.

Tréguer, P., Bowler, C., Moriceau, B., Dutkiewicz, S., Gehlen, M., Aumont, O., Bittner, L., Dugdale, R., Finkel, Z., Iudicone, D., Jahn, O., Guidi, L., Lasbleiz, M., Leblanc, K., Levy, M., and Pondaven, P.: Influence of diatom diversity on the ocean biological carbon pump, Nature Geosci, 11, 27–37, https://doi.org/10.1038/s41561-017-0028-x, 2018.

Tsekhovsky, Y. G.: Sedimentogenesis and geodynamics in the Cretaceous-Paleogene boundary at the epoch of continental peneplanation. Article 1. Central and Eastern Eurasia., pp. 5–23, 2015.

Tukey, J.: Exploratory data analysis, Addison-Wesley, 1977.

Tyrrell, T.: The relative influences of nitrogen and phosphorus on oceanic primary production, 400, 525–531, 1999.

Vahlenkamp, M., Niezgodzki, I., De Vleeschouwer, D., Lohmann, G., Bickert, T., and Pälike, H.: Ocean and climate response to North Atlantic seaway changes at the onset of long-term Eocene cooling, Earth Planet. Sci. Lett., 498, 185–195, https://doi.org/10.1016/j.epsl.2018.06.031, 2018.

Van Breedam, J., Huybrechts, P., and Crucifix, M.: Modelling evidence for late Eocene Antarctic glaciations, Earth and Planetary Science Letters, 586, 117 532, https://doi.org/10.1016/j.epsl.2022.117532, 2022.

Wade, B. S. and Pälike, H.: Oligocene climate dynamics, Paleoceanography, 19, 2004PA001 042, https://doi.org/10.1029/2004PA001042, 2004.

Wade, B. S., O'Neill, J. F., Phujareanchaiwon, C., Ali, I., Lyle, M., and Witkowski, J.: Evolution of deep-sea sediments across the Paleocene-Eocene and Eocene-Oligocene boundaries, Earth-Science Reviews, 211, 103 403, https://doi.org/10.1016/j.earscirev.2020.103403, 2020.

Westerhold, T., Marwan, N., Drury, A. J., Liebrand, D., Agnini, C., Anagnostou, E., Barnet, J. S. K., Bohaty, S. M., De Vleeschouwer, D., Florindo, F., Frederichs, T., Hodell, D. A., Holbourn, A. E., Kroon, D., Lauretano, V., Littler, K., Lourens, L. J., Lyle, M., Pälike, H., Röhl, U., Tian, J., Wilkens, R. H., Wilson, P. A., and Zachos, J. C.: An astronomically dated record of Earth's climate and its predictability over the last 66 million years, Science, 369, 1383–1387, https://doi.org/10.1126/science.aba6853, 2020.

Witkowski, J.: Early Paleocene-Late Eocene diatoms from the Blake Nose, western North Atlantic Ocean., vol. 152 of *Nova Heidwigia, Beiheft*, J. CRAMER Borntraeger Science Publishers, 2022.

Witkowski, J., Penman, D. E., Bryłka, K., Wade, B. S., Matting, S., Harwood, D. M., and Bohaty, S. M.: Early Paleogene biosiliceous sedimentation in the Atlantic Ocean: Testing the inorganic origin hypothesis for Paleocene and Eocene chert and porcellanite, Palaeogeogr. Palaeoclimatol. Palaeoecol., 556, 109 896, https://doi.org/10.1016/j.palaeo.2020.109896, 2020.

Witkowski, J., Bryłka, K., Bohaty, S. M., Mydłowska, E., Penman, D. E., and Wade, B. S.: North Atlantic marine biogenic silica accumulation through the early to middle Paleogene: implications for ocean circulation and silicate weathering feedback, Clim. Past, 17, 1937–1954, https://doi.org/10.5194/cp-17-1937-2021, 2021.

Yanchilina, A., Yam, R., Kolodny, Y., and Shemesh, A.: From diatom opal-A δ18O to chert δ18O in deep sea sediments, Geochimica et Cosmochimica Acta, 268, 368–382, https://doi.org/10.1016/j.gca.2019.10.018, 2020.

Zachos, J., Pagani, M., Sloan, L., Thomas, E., and Billups, K.: Trends, Rhythms, and Aberrations in Global Climate 65 Ma to Present, Science, 292, 686–693, https://doi.org/10.1126/science.1059412, 2001.

Zahajská, P., Opfergelt, S., Fritz, S. C., Stadmark, J., and Conley, D. J.: What is diatomite?, Quat. res., 96, 48–52, https://doi.org/10.1017/qua.2020.14, 2020.
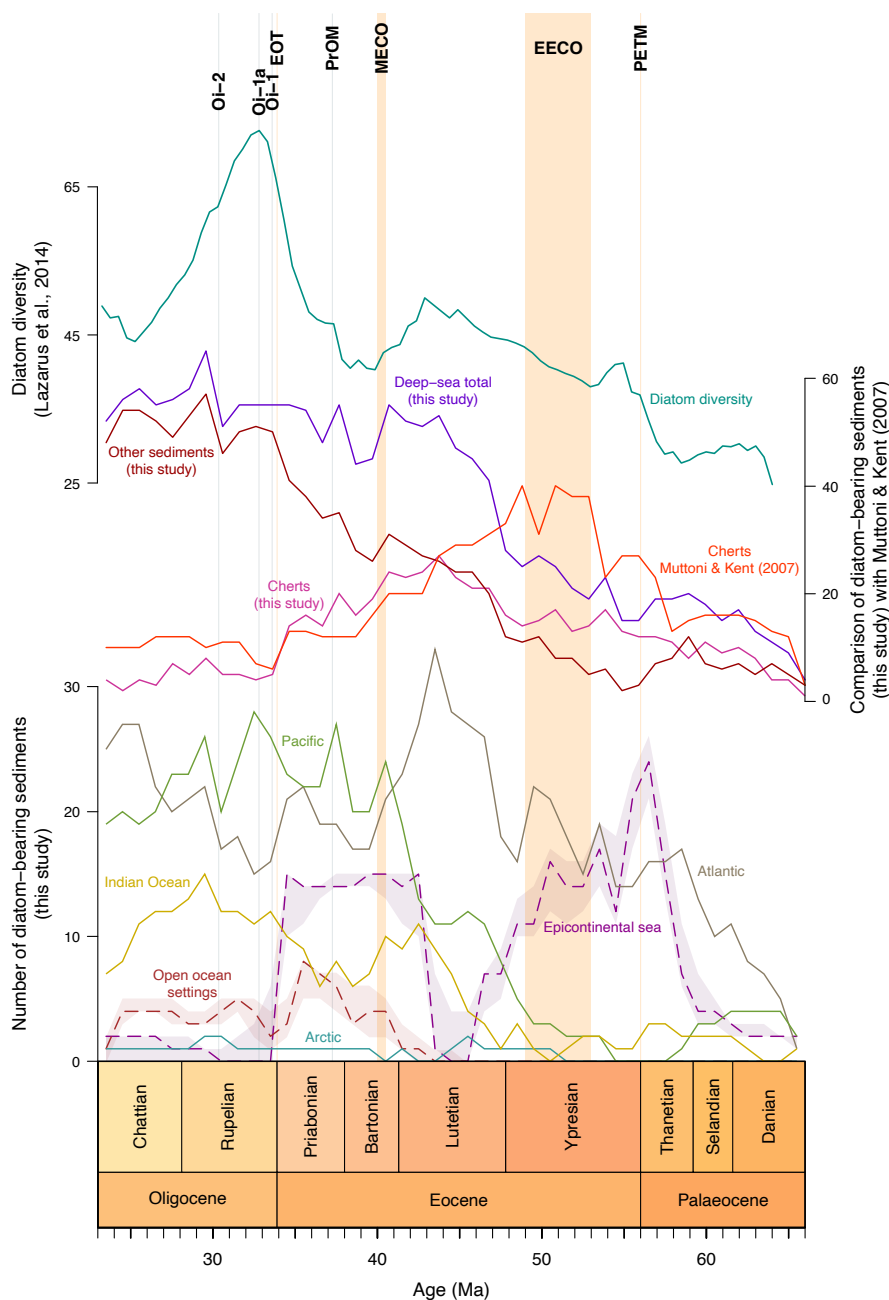
Figure 1. Comparison between our data and shallow marine diatomites (Figus et al., 2024a), cherts (Muttoni and Kent, 2007)and diatom diversity (Lazarus et al., 2014) distributions through the Palaeogene.
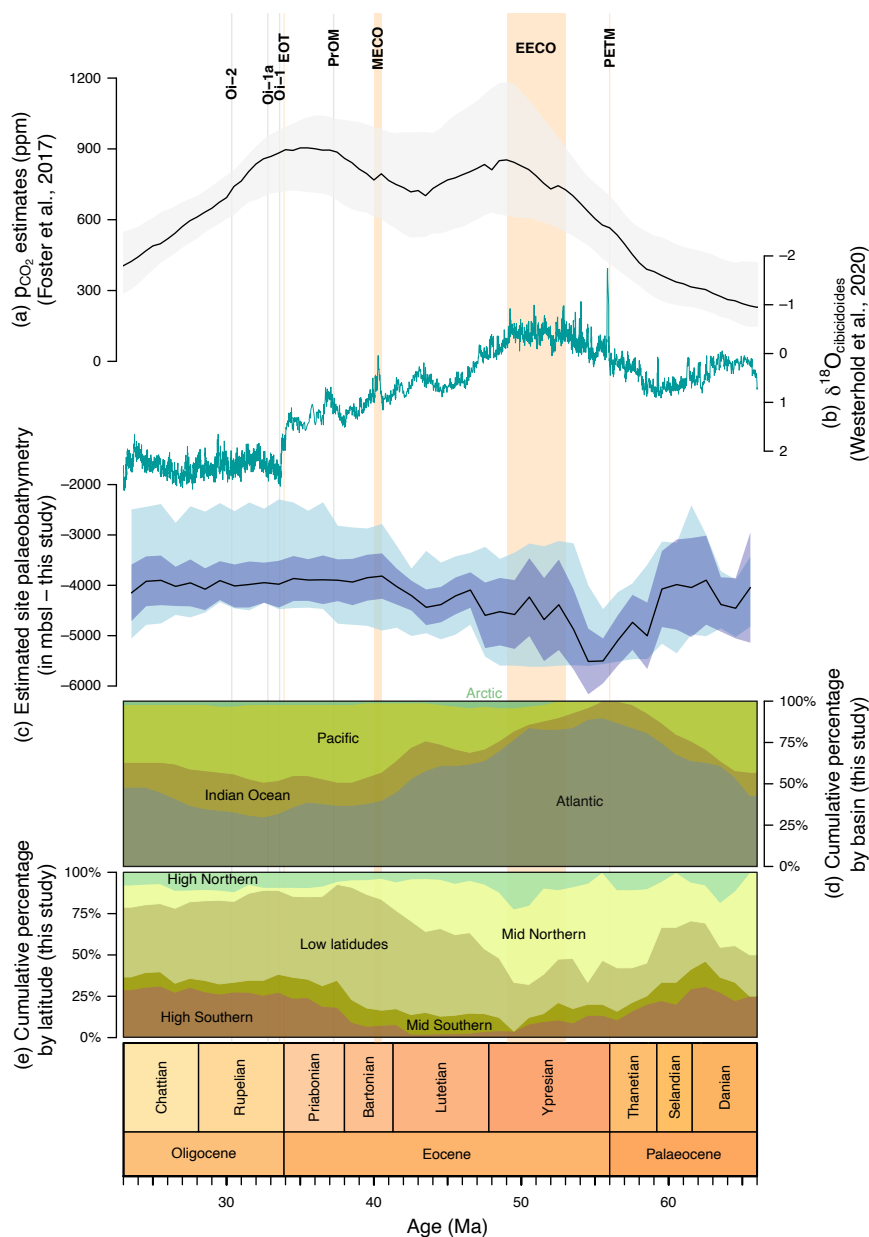
Figure 2. Comparison between our data and various proxies. (a) p_{CO_2} estimates from Foster et al. (2017), with mean in black and 95% confidence interval in grey; (b) $\delta^{18}O_{Cibicidoides}$ from Westerhold et al. (2020); (c) median estimated site palaeobathymetry (msbl) with 95% confidence interval on the median (McGill et al., 1978; in dark blue) and interquartile range (Tukey, 1977; in lighter blue); (d) cumulative percentage of diatom-bearing sediment occurrences by basin (this study); (e) cumulative percentage of diatom-bearing sediment occurrences by palaeolatitude (this study), with limits defined from -90° to -45° and from 90° to 45° for the high latitudes, from -45° to -30° and 45° to 30° for the mid latitudes, and from -30° to 30° for the low latitudes.
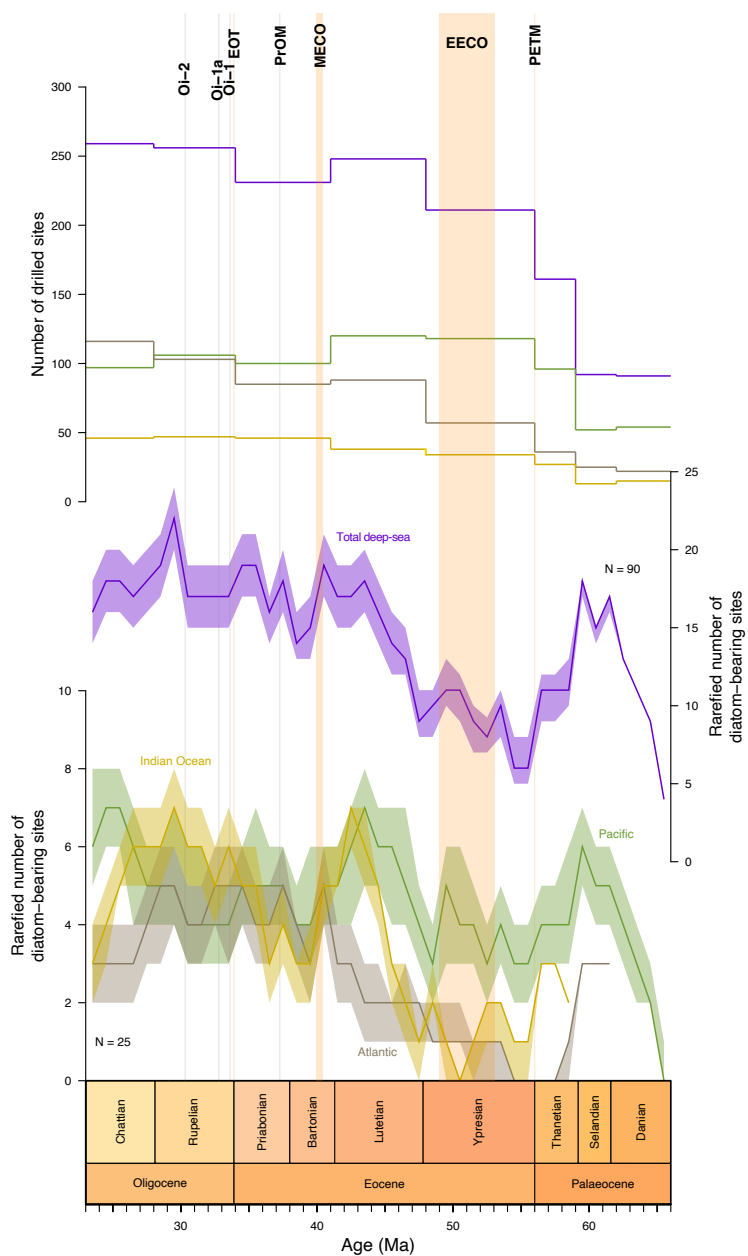
Figure 3. Correction of the sampling bias related to the number of drilled sites.
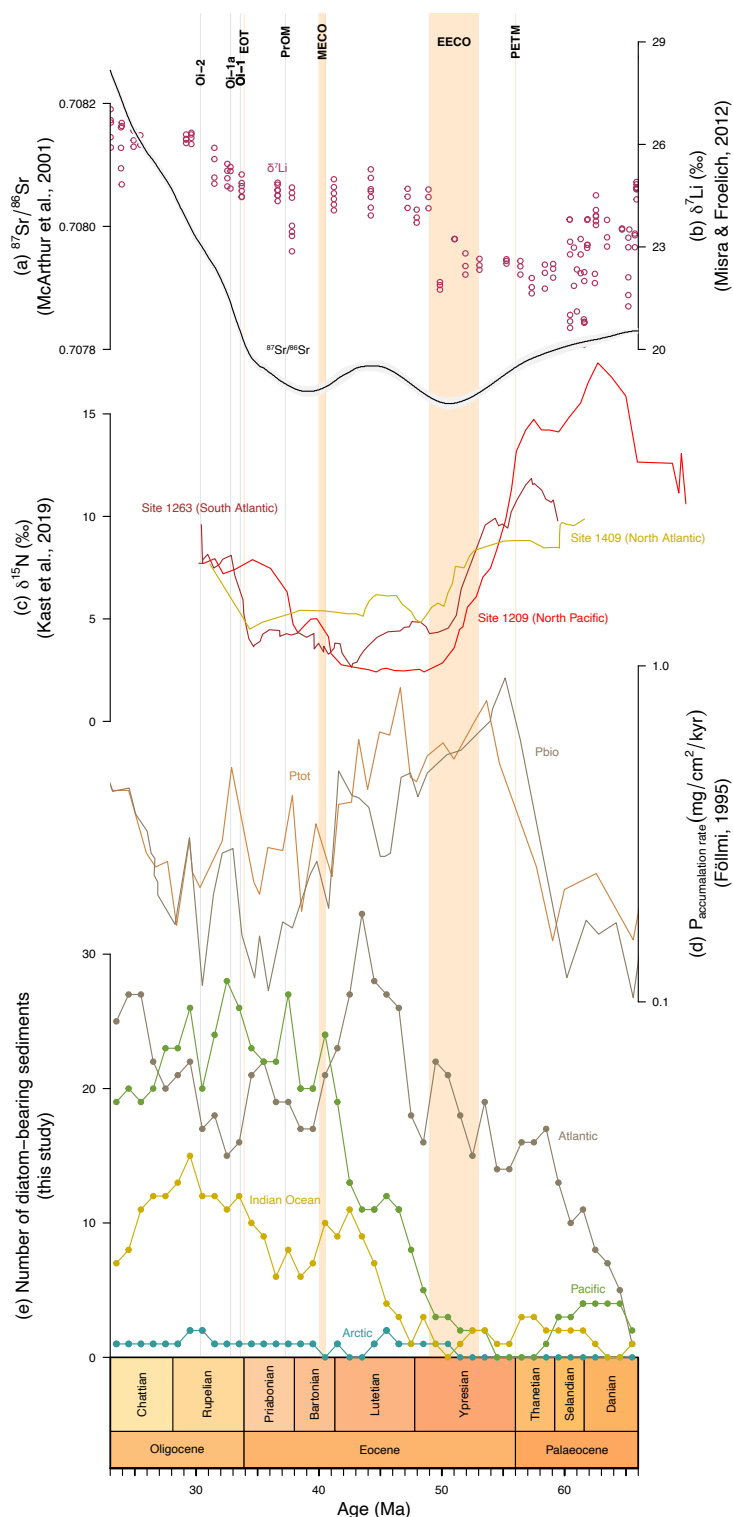
Figure 4. Comparision between the number of diatom-bearing sediments and various proxies. (a) ^{87}Sr/^{86}Sr from McArthur et al. (2001); (b) δ^7Li (‰) from Misra and Froelich (2012), (c) δ^{15}N (‰) from Kast et al. (2019); (d) accumulation rate of phosphorus (P) in $mg.cm^{-2}.kyr^{-1}$ from Föllmi (1995), with P_{tot} representing all types of phosphate sediments and P_{bio} the sediments containing bioavailable phosphorus only; (e) number of diatom-bearing sediments by basin (this study).
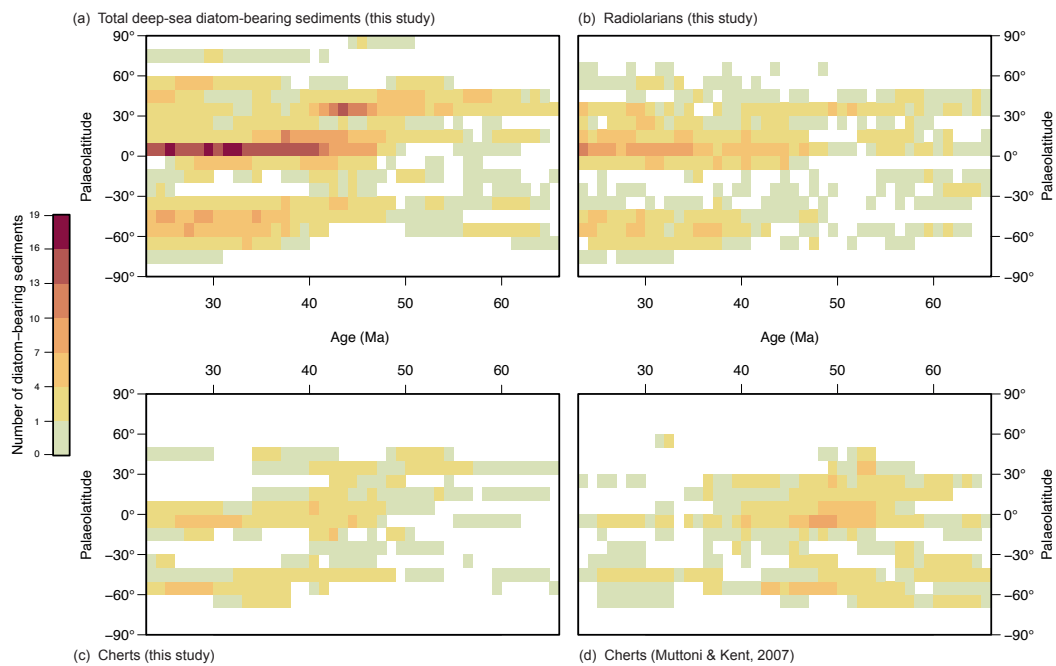
Figure 5. Comparison between the distribution of (a) total deep-sea diatom-bearing sediments (this study); (b) radiolarians (this study); (c) cherts from this study and (d) cherts from Muttoni and Kent (2007); by palaeolatitudes.